Video Article

TiO_2-coated Hollow Glass Microspheres with Superhydrophobic and High IR-reflective Properties Synthesized by a Soft-chemistry Method

Yinting Wong[1], Dan Zhong[2], Aotian Song[4], Yan Hu[3]

[1]Department of Biomedical Science, City University of Hong Kong

[2]Technological and Higher Education Institute of Hong Kong

[3]Hong Kong Polytechnic University

[4]Pavotech Co. Ltd.

Correspondence to: Aotian Song at songaotian1791@126.com, Yan Hu at huyan900719@gmail.com

URL: https://www.jove.com/video/55389
DOI: doi:10.3791/55389

Keywords: Chemistry, Issue 122, TiO_2, hollow glass microspheres (HGM), super hydrophobicity, infrared (IR) reflectivity, X-ray diffraction (XRD), scanning electron microscopy (SEM), energy-dispersive detector (EDS)

Date Published: 4/26/2017

Citation: Wong, Y., Zhong, D., Song, A., Hu, Y. TiO_2-coated Hollow Glass Microspheres with Superhydrophobic and High IR-reflective Properties Synthesized by a Soft-chemistry Method. *J. Vis. Exp.* (122), e55389, doi:10.3791/55389 (2017).

Abstract

This manuscript proposes a soft-chemistry method to develop superhydrophobic and highly IR-reflective hollow glass microspheres (HGM). The anatase TiO_2 and a superhydrophobic agent were coated on the HGM surface in one step. TBT and PFOTES were selected as the Ti source and the superhydrophobic agent, respectively. They were both coated on the HGM, and after the hydrothermal process, the TBT turned to anatase TiO_2. In this way, a PFOTES/TiO_2-coated HGM (MCHGM) was prepared. For comparison, PFOTES single-coated HGM (F-SCHGM) and TiO_2 single-coated HGM (Ti-SCHGM) were synthesized as well. The PFOTES and TiO_2 coatings on the HGM surface were demonstrated through X-ray diffraction (XRD), scanning electron microscopy (SEM), and energy-dispersive detector (EDS) characterizations. The MCHGM showed a higher contact angle (153°) but a lower sliding angle (16°) than F-SCHGM, with a contact angle of 141.2° and a sliding angle of 67°. In addition, both Ti-SCHGM and MCHGM displayed similar IR reflectivity values, which were about 5.8% higher than the original HGM and F-SCHGM. Also, the PFOTES coating barely changed the thermal conductivity. Therefore, F-SCHGM, with a thermal conductivity of 0.0479 W/(m·K), was quite like the original HGM, which was 0.0475 W/(m·K). MCHGM and Ti-SCHGM were also similar. Their thermal conductivity values were 0.0543 W/(m·K) and 0.0543 W/(m·K), respectively. The TiO_2 coating slightly increased the thermal conductivity, but with the increase in reflectivity, the overall heat-insulation property was enhanced. Finally, since the IR-reflecting property is provided by the HGM coating, if the coating is fouled, the reflectivity decreases. Therefore, with the superhydrophobic coating, the surface is protected from fouling, and its lifetime is also prolonged.

Video Link

The video component of this article can be found at https://www.jove.com/video/55389/

Introduction

Hollow glass microspheres (HGM) are inorganic materials ranging in size from 10 to 100 μm. They demonstrate many useful features, such as excellent dispersion, high flow ability, low density, and superior thermal insulation properties[1,2,3,4]. Because of their hollow structure, HGM have an extremely low thermal conductivity[10,11]. For these reasons, they are applied in many areas, including aerospace engineering[5], deep-sea exploration[6,7], hydrogen storage[8,9], *etc.* However, they still demonstrate some disadvantages, such as low strength. In addition, IR light is able to transmit through HGM and heat the subject behind. Therefore, surface modifications on HGM are essential to reduce the radiative thermal transfer. An effective method is to coat an IR-blocking material onto the HGM surface. As a semiconductor, TiO_2 has been used in many areas, such as photo-catalysis[12,13], solar cell development, sensor fabrication[14], environmental applications[15], and energy storage[16]. In addition, it also shows low emissivity in the visible light and infrared band[17,18,19]. Therefore, for our purposes, TiO_2 was a prudent selection due to its relatively low price and high performance.

However, the coating is quite easy for pollutants to foul, which seriously affects the reflectivity of TiO_2. The reflectivity must reduce gradually. Therefore, a self-cleaning coating is essential to prevent the coating from fouling and to prolong the working time of such a coating.

In this manuscript, a soft-chemistry method was used to develop superhydrophobic TiO_2-coated HGM. Tetrabutyl titanate (TBT) and 1H,1H,2H,2H-perfluorooctyltriethoxysilane (PFOTES) were selected as the Ti source and superhydrophobic agent, respectively. They were hydrolyzed and deposited on the HGM surface. Then, after the hydrothermal process, the anatase TiO_2 formed on the HGM surface, and the superhydrophobic properties remained. For comparison, PFOTES single-coated HGM (F-SCHGM) and TiO_2 single-coated HGM (Ti-SCHGM) were synthesized as well. The synthesis scheme is shown in **Figure 1**.

Copyright © 2017 Journal of Visualized Experiments

Protocol

1. Pre-treatment of HGM

1. Place the HGM into a 500-mL beaker with 200 mL of absolute alcohol; the low density of unbroken HGM causes it to suspend in the alcohol, but because the density of broken HGM is larger than that of alcohol, it precipitates in the solution. After 30 min, collect the suspended HGM using a clean spoon and dry at 80 °C in an oven for further application.

2. Synthesis of MCHGM

1. Place 5 g of unbroken HGM, 47.5 mL of ethanol, and 2.5 mL of DI water in a three-necked flask. Stir using a mixing motor at 400 r/min for 20 min (pre-mixing).
2. Mix **15 g of TBT, 1 g of PFOTES**, and 30 mL of absolute alcohol in a 200-mL beaker. Pour the mixture into a constant-pressure funnel.
3. Insert the constant-pressure funnel into one of the holes of the three-necked flask. Drop the mixture contained in the constant-pressure funnel into the three-necked flask at a speed of 1 drop per 7 s, which is achieved by adjusting the valve of the constant-pressure funnel. Continue the reaction for 3 h.
4. Pour the mixture from the three-necked flask into a hydrothermal reactor. Put the sealed reactor in a suitable steel sleeve in a 180 °C oven for 6 h.
   NOTE: Make sure that the reactor has a suitable cover. After it is covered, put the reactor into the steel sleeve. The sleeve should also be sealed with a cover.
5. After the reaction is over, collect the samples suspended in the hydrothermal reactor using a big spoon. Dry the samples at 80 °C for 4 h to obtain **MCHGM**.

3. Synthesis of F-SCHGM

1. Add 5 g of unbroken HGM, 47.5 mL of absolute ethanol, and 2.5 mL of DI water to a three-necked flask. Stir using a mixing motor at 400 r/min for 20 min (pre-mixing). Mix **1 g of PFOTES** and 30 mL of absolute ethanol in a 200-mL beaker. Transfer the PFOTES and absolute ethanol mixture to a constant-pressure funnel.
2. Insert the constant-pressure funnel into the three-necked flask. Drop the mixture contained in the constant-pressure funnel into the three-necked flask at a speed of 1 drop per 7 s. Let the reaction run for 3 h.
3. Transfer the mixture from the three-necked flask to a hydrothermal reactor. Put the sealed reactor in a 180 °C oven for 6 h. After the reaction is over, collect the samples suspended in the hydrothermal reactor using a big spoon. Dry the samples at 80 °C for 4 h to obtain **F-SCHGM**.

4. Synthesis of Ti-SCHGM

1. Place 5 g of unbroken HGM, 47.5 mL of absolute ethanol, and 2.5 mL of DI water in a three-necked flask. Stir at 400 r/min for 20 min (pre-mixing). Mix **15 g of TBT** and 30 mL of absolute ethanol in a 200-mL beaker. Transfer the TBT and absolute ethanol mixture to a constant-pressure funnel.
2. Insert the constant-pressure funnel into the three-necked flask. Drop the mixture in the constant-pressure funnel into the three-necked flask at a speed of 1 drop per 7 s. Let the reaction run for 3 h.
3. Transfer the mixture from the three-necked flask to a hydrothermal reactor. Put the sealed reactor in a 180 °C oven for 6 h. Collect the samples in the hydrothermal reactor after the reaction is over. Dry the samples at 80 °C for 4 h to obtain **Ti-SCHGM**.

5. Characterizations

1. Conduct XRD characterizations on all samples. Collect the data using a highly versatile, multipurpose X-ray diffraction system with Cu Kα radiation (λ = 0.15406 nm) and a 2θ ranging from 10° to 80°.
2. Acquire scanning electron microscope[20,21] images after spraying the samples with gold. During the SEM tests, conduct the EDS is on a specific area.
3. Measure the contact angle by using a contact-angle goniometer[22]; the water drop volume should be 10 μL.
4. Measure the sliding angle[23] by changing the tilt angle of the surface. Minimize the angle until the water drop can just slide down.
   1. Stick double-sided tape on a glass sheet (size: 26 mm x 76 mm x 2 mm). Using a spoon, uniformly place the powders (F-SCHGM or MCHGM) on the tape. Using an injector, add a water drop (volume: 0.05 mL) to the powder surface.
   2. Put the glass sheet on the motor platform of the contact-angle goniometer. Tilt the glass sheet by leaning the motor platform at a rate of 1°/s. Stop the motor when the water drop starts to slide; the tilt angle is the sliding angle.
5. Measure the reflectivity spectra using a spectrophotometer[24]. NOTE: The wavelength is from 450 nm to 2,550 nm.
6. Measure the thermal conductivity of all samples using a thermal conductivity meter[25].

Copyright © 2017 Journal of Visualized Experiments

Representative Results

The tests in step 4.4 reveal many features and properties of the samples. The XRD (**Figure 2**) reflects the formation of anatase TiO_2. The SEM (**Figure 3**) and EDS (**Figure 4**) display the TiO_2 and PFOTES that are coated on the HGM surface. The contact angle (**Figure 5**) and sliding angle (**Figure 6**) tests represent the superhydrophobicity. The Vis-NIR transmittance test (**Figure 8**) describes the reflective properties of the TiO_2 coating, and the thermal conductivity (**Figure 9**) demonstrates that the coating does not increase the thermal conductivity.

As shown in **Figure 2**, the four samples undergo the XRD tests. The broad peak at around 2θ = 23° represents the amorphous SiO_2, which is the main component of HGM. This peak is detected in the four samples, which demonstrates the existence of HGM. Since PFOTES is the only coating with a thickness of a few molecules, it does not change the XRD signal. Therefore, the XRD patterns of the original HGM, F-SCHGM, Ti-SCHGM, and MCHGM are almost the same. As for Ti-SCHGM and MCHGM, besides the broad peak of SiO_2, the other peaks ((101), (004), (200), (105), (211), (213), and (204)) are perfectly indexed to the standard TiO_2 (PDF#89-4921). This reflects that the anatase TiO_2 is formed in the final products.

The SEM images are shown in **Figure 3**. As shown in those images, the F-SCHGM and the original HGM have no difference on the surface because the PFOTES coating is only a few molecules thick. For MCHGM and Ti-SCHGM, it is quite obvious that there are coatings on the surface. The EDS results are shown in **Figure 4**. The pink area in **Figure 3** was investigated by EDS. As shown in **Figure 4a**, only Si, O, Na, and Ca were detected. In **Figure 4b**, besides these four elements, F is also detected. This is the characterization element of PFOTES, which was revealed to be coated on the HGM surface. In **Figure 4c**, besides the four elements in **Figure 4a**, Ti was detected, which indicates that TiO_2 is coated on the HGM. In **Figure 4d**, besides the five elements in **Figure 4c**, F was also detected. This demonstrates that both TiO_2 and PFOTES are coated on the HGM surface.

The contact angle was then investigated. As shown in **Figure 5**, the contact angles of the original HGM (**Figure 5a**), F-SCHGM (**Figure 5b**), Ti-SCHGM (**Figure 5c**), and MCHGM (**Figure 5d**) are 59°, 141.2°, 85°, and 153°, respectively. With the help of PFOTES, the contact angles of F-SCHGM and MCHGM both exhibit a huge increase. However, their sliding angles (**Figure 6**) are different. The sliding angles of F-SCHGM and MCHGM are 67° and 16°, respectively. This is because of the special structure formed by TiO_2 on HGM. This special structure increases the surface roughness, so the sliding angle is also changed. The Cassie-Baxter wetting model[26], shown in **Figure 7**, is able to explain the superhydrophobic phenomenon. Formula 1 describes this model. In this formula, θ^c is the apparent contact angle, θ is Young's contact angle[27], and f is the solid-phase fraction. With the help of TiO_2, both the roughness of the HGM surface and the f-value are increased. Therefore, the contact angle became bigger. The TiO_2 coating helped to form the pillar structure on the HGM surface. Therefore, the water drop is supported by an air mat, and, when sliding, the resistance is smaller. Thus, the sliding angle of MCHGM is smaller.

$$\cos\theta^c = f\cos\theta - (1 - f) \quad (1)^{26}$$

The reflectivity was then investigated and shown in **Figure 8**. Since the PFOTES coating barely changes the reflectivity, those four samples were divided into two groups. The first one is the original HGM and F-SCHGM, and the second one is the Ti-SCHGM and MCHGM. In each group, the data of reflectivity are quite similar. However, with the help of TiO_2, the reflectivity increased by 5%.

Finally, the influence of the TiO_2 coating on the thermal conductivity was investigated. This is essential because the TiO_2 coating increases the wall thickness of HGM. Thus, the thermal conductivity of TiO_2-coated HGM is a little bit higher than uncoated HGM. However, the thermal conductivity enhancement should not be so obvious that the overall heat insulation property weakens. As shown in **Figure 9**, since the PFOTES barely changed the thermal conductivity, only TiO_2 contributed to the gains in this parameter. However, the increase was limited. The thermal conductivities of the original HGM, F-SCHGM, Ti-SCHGM, and MCHGM were 0.0475 W/(m·K), 0.0479 W/(m·K), 0.0546 W/(m·K), and 0.0543 W/(m·K), respectively. Thus, even though the TiO_2 coating increased the thermal conductivity due to the gain in HGM wall thickness, the increase was slight. The overall thermal insulation properties of such TiO_2-coated HGM were improved by the reflectivity enhancement that derived from the TiO_2.

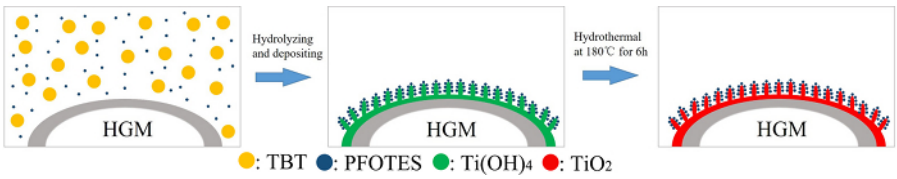

Figure 1: The synthesis scheme of MCHGM. For other samples, such as F-SCHGM and Ti-SCHGM, the processes are quite similar, but without related raw materials. Please click here to view a larger version of this figure.

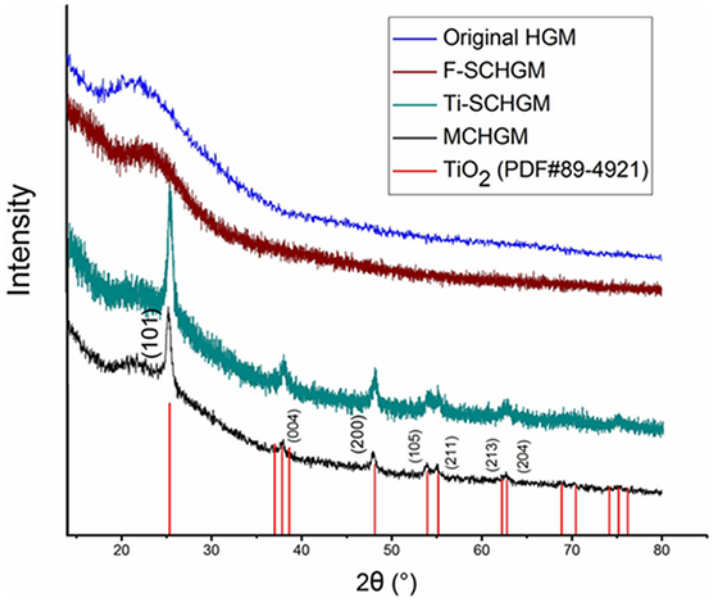

Figure 2: The XRD spectra of the original HGM, superhydrophobic TiO2/HGM, and standard anatase TiO_2. The spectra were detected by a highly versatile, multipurpose X-ray diffraction system with Cu Kα radiation (λ = 0.15406 nm) and a 2θ ranging from 10° to 80°. There are no obvious differences between the original HGM and F-SCHGM or Ti-SCHGM and MCHGM. Please click here to view a larger version of this figure.

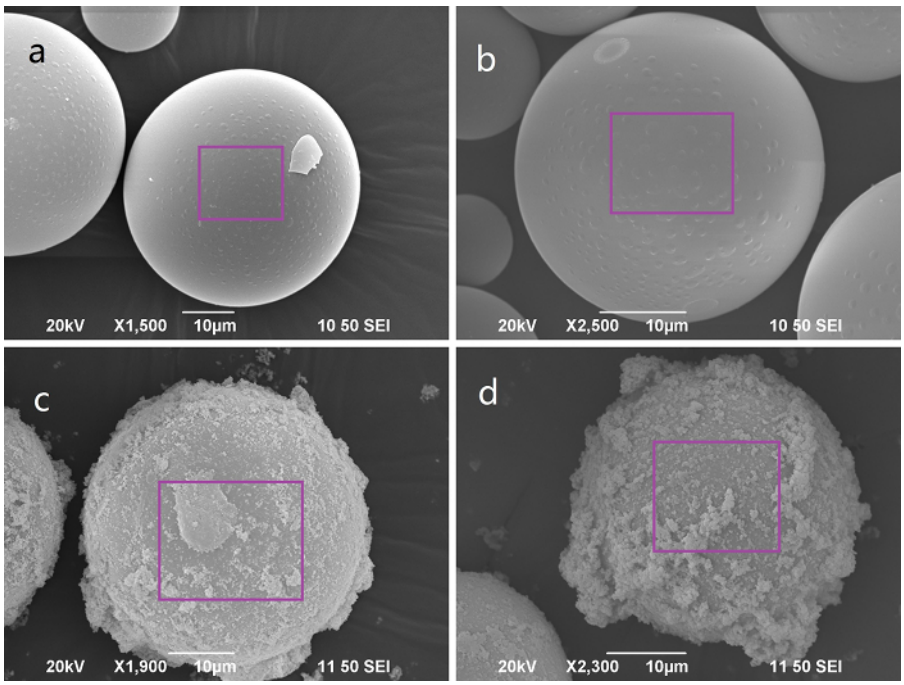

Figure 3: The morphology of (a) the original HGM, (b) F-SCHGM, (c) Ti-SCHGM, and (d) MCHGM, detected using a scanning electron microscope. On the original HGM and F-SCHGM surfaces, the coatings cannot be observed via SEM, but coatings do exist on the surfaces of Ti-SCHGM and MCHGM. Please click here to view a larger version of this figure.

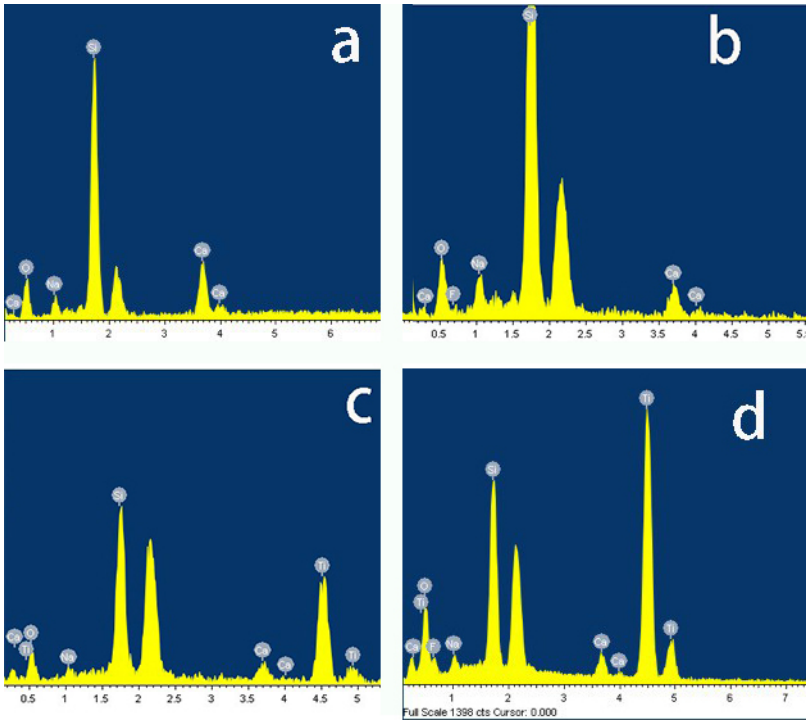

Figure 4: The EDS measurements of the red-framed areas of (a) the original HGM, (b) F-SCHGM, (c) Ti-SCHGM, and (d) MCHGM, detected using a scanning electron microscope. The characteristic elements of PFOTES and TiO_2 were detected.

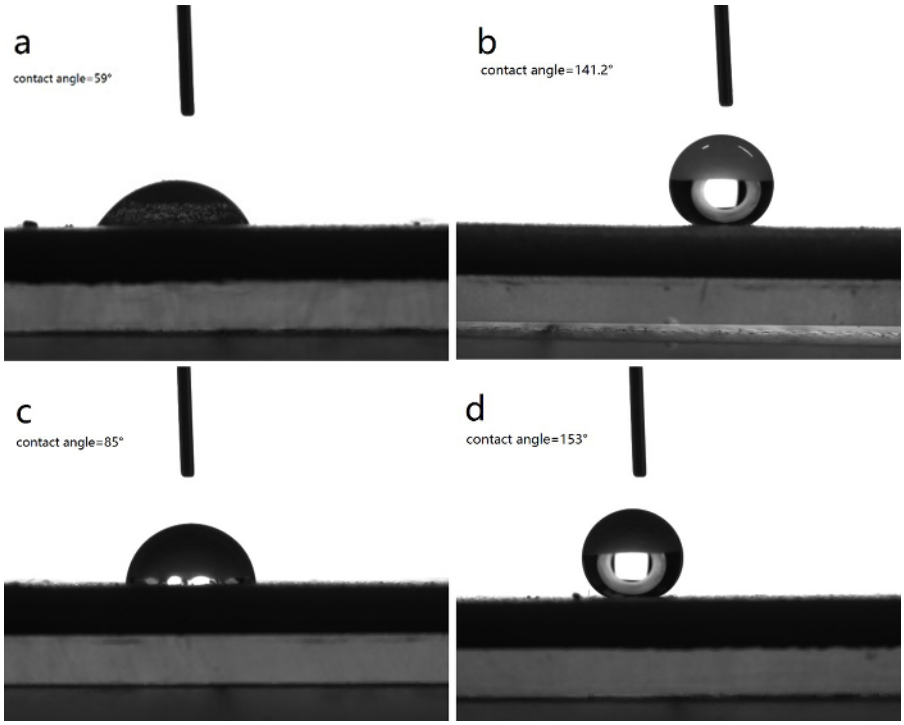

Figure 5: The contact angle of (a) the original HGM, (b) F-SCHGM, (c) Ti-SCHGM, and (d) MCHGM are detected by the contact-angle goniometer. With the help of PFOTES, the contact-angle values of F-SCHGEM and MCHGM show a great increase. Please click here to view a larger version of this figure.

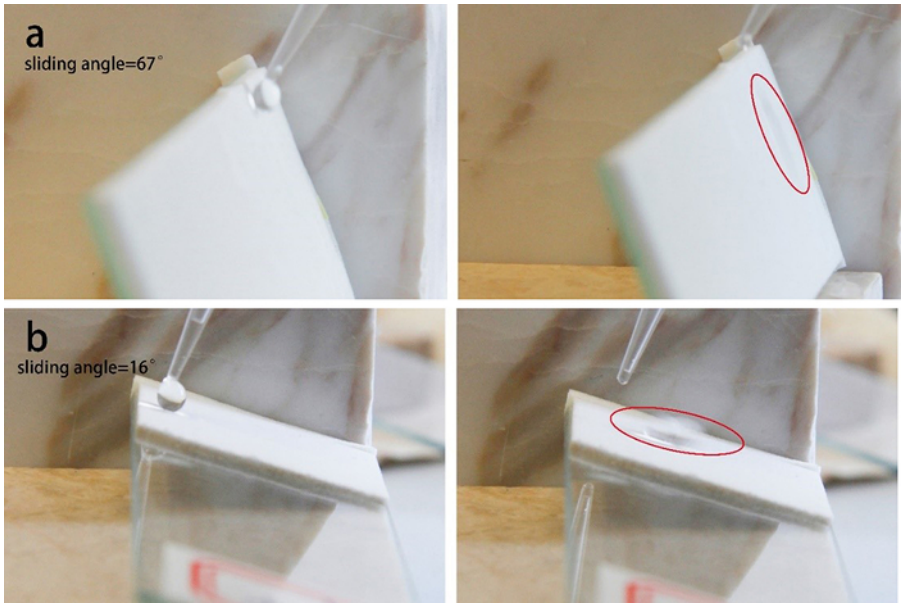

Figure 6: The sliding angle of (a) F-SCHGM and (b) MCHGM. The red circle marks the sliding path of the water drop. MCHGM shows a lower sliding angle. Please click here to view a larger version of this figure.

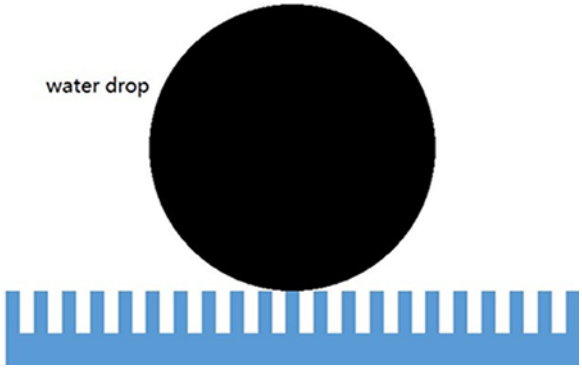

Figure 7: The Cassie-Baxter wetting theory of superhydrophobicity. This is the model that describes wetting theory. The black circle represents the water drop. The little pillars represent the rough surface.

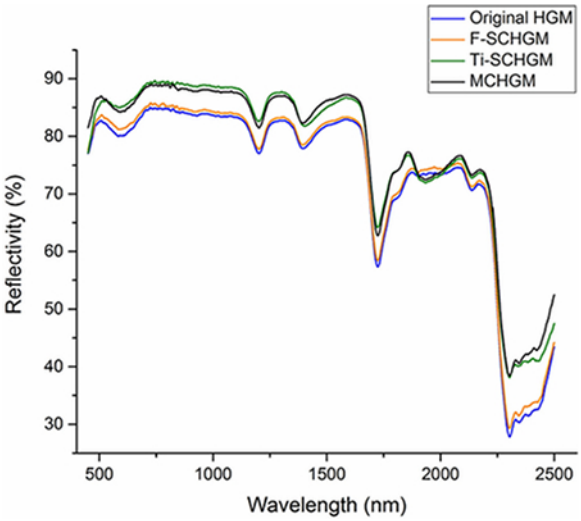

Figure 8: The reflectivity spectra of the original HGM, F-SCHGM, Ti-SCHGM, and MCHGM, detected by the spectrophotometer. The TiO_2-coated HGM shows better reflectivity than the original HGM. Please click here to view a larger version of this figure.

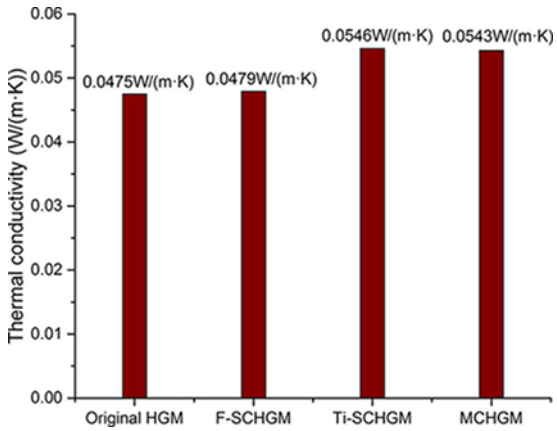

Figure 9: The thermal conductivity of the four samples, detected by a thermal conductivity meter. The increase in thermal conductivity derives from the gain in wall thickness. Please click here to view a larger version of this figure.

Discussion

In this manuscript, the critical step in the protocol is the hydrothermal process. It influences the formation of TiO_2, the final reflectivity, and the superhydrophobicity. The temperature control and reaction time are also quite significant. If the reaction conditions change, the final products can be flawed.

This method provides a simple way to synthesize superhydrophobic and highly IR-reflective HGM in one step. In previous research, the superhydrophobic and reflectivity properties were achieved by separate means[28,29,30]. Therefore, to obtain both, at least two steps are required. In this manuscript, a one-step method is proposed, largely enhancing the production efficiency. Also, with those two properties combined, the IR-reflective coating is protected from fouling, and the coating performance can be retained for a long time.

However, there is a limitation in terms of large-scale synthesis. This method should be further modified for such purposes. When it comes to a large hydrothermal reactor, the heat and mass transfer must be well-organized.

This technique is significant when compared to existing methods because it allows for the synthesis of superhydrophobic and highly IR-reflective HGM in one step. The coating is the key factor for reflecting the IR. Thus, it is also quite important to keep the surface clean. With the superhydrophobic self-cleaning property, the coating can be protected from fouling, and the lifetime can be prolonged. In addition, because two steps are reduced to one step, the energy consumed during production is also reduced.

The proposed technique demonstrated in this manuscript represents a good method to synthesize a heat insulation material with a wide variety of applications. The superhydrophobic property is combined with other properties, such as IR-reflection. Therefore, if necessary, the superhydrophobic synthesis method can be applied to other functional materials, such as IR-absorption materials[31], anti-corrosion materials[32] or even solar cells[33].

Disclosures

The authors have nothing to disclose.

Acknowledgements

The work described in this paper was supported by a grant from the CII-HK/PolyU Innovation Fund. Further support was provided by the Shenzhen Peacock Plan (KQTD2015071616442225) and the Chinese Government "Thousand Talent" Program (Y62HB31601). Also, the help from the Department of Applied Biology & Chemical Technology of the Hong Kong Polytechnic University and the Hong Kong Polytechnic University Research Institute for Sustainable Urban Development (RISUD) is appreciated.

References

1. Yung, K.C., Zhu, B.L., Yue, T.M., Xie, C.S. Preparation and properties of hollow glass microsphere-filled epoxy-matrix composites. *Compos. Sci. Technol.* **69** (2): 260-264 (2008).
2. Xu, N., Dai, J., Zhu, Z., Huang, X., Wu, P. . Synthesis and characterization of hollow glass-ceramics microspheres. *Compos. Sci. Technol.* 72 (4): 528-532 (2011).
3. Li, B., Yuan, J., An, Z., Zhang, J. Effect of microstructure and physical parameters of hollow glass microsphere on insulation performance. *Mater. Lett.* **65** (12), 1992-1994 (2011).
4. Hu, Y., Mei, R., An, Z., *et al.* Silicon rubber/hollow glass microsphere composites: Influence of broken hollow glass microsphere on mechanical and thermal insulation property. *Compos. Sci. Technol.* 79: 64-69. (2013).
5. Geleil, A.S., Hall, M.M., Shelby, J.E. Hollow glass microspheres for use in radiation shielding. *J. Non-Cryst. Solids.* **352,** 620-625 (2006).
6. Khimiya. *Handbook of Fillers for Polymeric Composite Materials [Russian translation].* Moscow (1981).

Copyright © 2017 Journal of Visualized Experiments

7. Greiner-Bar, G. HoNe Mikroglaskugeln. *Herstellung, Eigenschaften und Anwendung.* Silikattechnik., 40, No. 1, 23-25 (1989).
8. Kool, L.B., *Method for storing hydrogen, and related articles and systems.* United States Patent 7749304, (2010).
9. Brow Richard, K., Schmitt Melodie L. A survey of energy and environmental application of glass. *J. Eur. Ceram. Soc.* **29** 1193-1201. (2009).
10. Awaja, F., Arhatari, B.D. X-ray Micro Computed Tomography investigation of accelerated thermal degradation of epoxy resin/glass microsphere syntactic foam. *Composites Part A.* **40** (8), 1217-1222 (2009).
11. Wang, S., Luo, R., Ni, Y. Preparation and characterization of resin-derived carbon foams reinforced by hollow ceramic microspheres. *Mater. Sci. Eng., A.* **527** (15), 3392-3395 (2010).
12. Carp, O., Huisman, C.L., Reller, A. Photoinduced reactivity of titanium dioxide. *Prog. Solid State Chem.* **32** (1), 33-177 (2004).
13. Fujishima, A., Rao, T.N., Tryk, D.A. Titanium dioxide photocatalysis. *J. Photochem. Photobiol. C.* **1** (1), 1-21 (2000).
14. Fujishima, A. Electrochemical photolysis of water at a semiconductor electrode. *Nature.* **197**, 37-38 (1972).
15. Hoffmann, M.R., Martin, S.T., Choi, W., *et al.* Environmental applications of semiconductor photocatalysis. *Chem. Rev.* **95** (1), 69-96 (1995).
16. Chen, X., Mao, S.S. Titanium dioxide nanomaterials: synthesis, properties, modifications, and applications. *Chem. Rev.* **107** (7), 2891-2959. (2007).
17. Yuan, J., An, Z., Li, B., *et al.* Facile aqueous synthesis and thermal insulating properties of low-density glass/TiO2 core/shell composite hollow spheres. *Particuology.* **10** (4), 475-479 (2012).
18. Yan, H., Yuanhao, W., Hongxing, Y. TEOS/silane coupling agent composed double layers structure: A novel super-hydrophilic coating with controllable water contact angle value. *Appl. Energy.* (2015).
19. Wang, Y., Yang, H., Lu, L. Three-dimensional double deck meshlike dye-sensitized solar cells. *J. Appl. Phys.* **108** (6): 064510 (2010).
20. Wang, Y., Yang, H., Xu, H. DNA-like dye-sensitized solar cells based on TiO 2 nanowire-covered nanotube bilayer film electrodes. *Mater. Lett.* **64** (2), 164-166 (2010).
21. Wang, Y., Lu, L., Yang, H., *et al.* Development of high dispersed TiO2 paste for transparent screen-printable self-cleaning coatings on glass. *J. Nanopart. Res.* **15** (1), 1-6 (2013).
22. Kwok, D.Y., Neumann, A.W. Contact angle measurement and contact angle interpretation. *Adv. Colloid Interface Sci.* **81** (3), 167-249. (1999).
23. Pierce, E., Carmona, F.J., Amirfazli, A. Understanding of sliding and contact angle results in tilted plate experiments. *Colloids Surf., A.* **323** (1), 73-82. (2008).
24. Kim, W.S., Kim, T.H., Kim, E.S., *et al.* Microwave dielectric properties and far infrared reflectivity spectra of the (Zr0. 8Sn0. 2) TiO4 ceramics with additives. *Jpn. J. Appl. Phys.* **37** (9S): 5367 (1998).
25. Hasselman, D.P.H., Johnson, L. F. Effective thermal conductivity of composites with interfacial thermal barrier resistance. *J. Compos. Mater.* **21** (6), 508-515 (1987).
26. Cassie, A.B.D., Baxter, S. Wettability of porous surfaces. ***Trans. Faraday Soc.*.** **40**, 546-551 1944 (1944).
27. Wenzel, R.N. Resistance of solid surfaces to wetting by water. *Ind. Eng. Chem. Res.* **28** (8), 988-994. (1936).
28. Shirtcliffe, N.J., McHale, G., Newton, M.I., *et al.* Intrinsically superhydrophobic organosilica sol-gel foams. *Langmuir.* **19** (14), 5626-5631. (2003).
29. Rothstein, J.P. Slip on superhydrophobic surfaces. *Annu. Rev. Fluid Mech.* **42**, 89-109. (2010).
30. Rodošek, M., Kreta, A., Gaberšček, M., *et al.* Ex situ IR reflection-absorption and in situ AFM electrochemical characterisation of the 1, 2-bis (trimethoxysilyl) ethane-based protective coating on AA 2024 alloy. *Corros. Sci.* **102**, 186-199. (2016).
31. Jiang, J., Zhang, J., Zhu, P., *et al.* High pressure studies of Ni 3 [(C 2 H 5 N 5) 6 (H 2 O) 6](NO 3) 6· 1.5 H 2 O by Raman scattering, IR absorption, and synchrotron X-ray diffraction. *RSC Adv.* **6** (69): 65031-65037. (2016).
32. Arukalam, I.O., Oguzie, E.E., Li, Y. Fabrication of FDTS-modified PDMS-ZnO nanocomposite hydrophobic coating with anti-fouling capability for corrosion protection of Q235 steel. Journal of Colloid and Interface *Science.* **484,** 220-228. (2016).
33. Hou, W., Xiao, Y., Han, G., *et al.* Serrated, flexible and ultrathin polyaniline nanoribbons: An efficient counter electrode for the dye-sensitized solar cell. *J. Power Sources.* **322**, 155-162 (2016).

Copyright © 2017 Journal of Visualized Experiments